

Non-myopic GOSPA-driven Gaussian Bernoulli Sensor Management

George Jones, Ángel F. García-Fernández, Christian Blackman

Abstract—In this paper, we propose an algorithm for non-myopic sensor management for Bernoulli filtering, i.e., when there may be at most one target present in the scene. The algorithm is based on selecting the action that solves a Bellman-type minimisation problem, whose cost function is the mean square generalised optimal sub-pattern assignment (GOSPA) error, over a future time window. We also propose an implementation of the sensor management algorithm based on an upper bound of the mean square GOSPA error and a Gaussian single-target posterior. Finally, we develop a Monte Carlo tree search algorithm to find an approximate optimal action within a given computational budget. The benefits of the proposed approach are demonstrated via simulations.

Index Terms—Non-myopic, sensor management, Monte Carlo search tree, Bernoulli filtering.

I. INTRODUCTION

CONDUCTING surveillance of a specified area can be completed by utilising autonomous vehicles which have a limited Field of View (FOV). This FOV is typically significantly smaller than the desired surveillance region and therefore the vehicle has to be agile in a way which allows it to alter the positioning of the FOV, allowing it to view adjacent areas. This can be visualised as an autonomous ground vehicle traversing the ground in search of aerial targets [12]. Other work was completed in [16] looking at search-detect-track sensor management for geosynchronous space objects. The discipline that plans which actions the sensor/vehicle should take at each time-step to achieve an objective of interest, such as the tracking of these aerial targets, is referred to as sensor management [27], [29].

In this paper, we deal with sensor management for Bernoulli filtering [38], in which, at any given time-step, a maximum of one target can be present. In a Bernoulli filter, a target is born, then moves with a certain dynamic model, and then disappears from the surveillance area. Only once this target has disappeared, a new target may appear [22]. This target is observed through noisy measurements, which may contain clutter as well as target detections. [38]. In Bernoulli filtering, the posterior probability of target existence and the spatial density are propagated through the filtering recursion [36], [38].

G. Jones, A. F. García-Fernández and C. Blackman are with the Department of Electrical Engineering, and Electronics, University of Liverpool, Liverpool L69 3GJ, U.K (emails: {g.jones6, angel.garcia-fernandez, c.blackman}@liverpool.ac.uk). A. F. García-Fernández is also with the ARIES Research Centre, Universidad Antonio de Nebrija, Madrid, Spain. This work was supported by the EPSRC Centre for Doctoral Training in Distributed Algorithms EP/S023445/1 and Roke Manor Research Limited.

This paper deals with the problem of finding the optimal sequence of actions for an agile sensor platform to keep track of the current target until it disappears, and then search for a potential new target. In a model-based setting, this type of problem is usually posed as a Partially Observable Markov Decision Process (POMDP) which is a framework that allows for planning when the system state is observed with uncertainty [22], [44]. Another type of framework to solve sensor management problems is to use reinforcement learning (usually in combination with neural networks). In [32], a double deep Q network is used to conduct sensor management on a ground based telescope for space situational awareness. Reinforcement learning methods have also been used to approach multiple target tracking in [17], [35] and sensor management for single target tracking in [23]. These methods can achieve very high performance, but typically require long training times and may lack interpretability.

In this paper, we focus on POMDPs which have an interpretable methodology whose aim is to minimise a cost function (or maximise a reward function). The cost function can consider a single time-step ahead of the current time-step. This approach is referred to as myopic planning. Intuitively, there are limiting cases in which myopic planning cannot find a desirable solution, such as having to navigate around an obstacle that requires a multi-time step planning approach (non-myopic planning). We proceed to review the literature to address the sensor management problem.

A popular cost function for single-target tracking is the posterior Cramér-Rao lower bound (PCRLB) [45]. The PCRLB has been applied to single-target tracking problems dealing with cluttered environments in [21] and multiple-targets for multisensor array management in [43]. It has also been used to develop a cognitive radar framework for target detection and tracking in [4] and used for extended target tracking in [42]. The PCRLB is a bound on the mean square error. The PCRLB is used instead of the mean square error due to its good performance and the fact that it is computationally efficient to calculate. As the PCRLB is a bound on the mean square error, using it as a cost function must incorporate external criteria to be able to carry out tracking of an unknown and varying number of targets.

Another method is to use a cost function based on information theory. Information-theoretic methods aim to select the action that maximises the expected information gain between the predicted and posterior density. Their objective is to take the action that gives the most information about the variables of interest. The information gain is measured by an information theoretic divergence, such as the Kullback-

Leibler (KL) divergence or the Rényi divergence [1], [3], [26], [28], [37], [40]. Whilst these approaches can lead to desirable results, it is not explicitly clear what the resulting policy is aiming for in terms of more practical aspects of multiple target-tracking.

The non-myopic case of sensor management considers the longer term impact of the actions that are chosen now [25]. The ability to plan further into the future, whilst offering many benefits, also carries some drawbacks. Building non-myopic sensor management algorithms for POMDP's can be challenging as the state is not fully observable, meaning both the state of the target and state of the sensor have to be updated without knowing whether or not an observation will be received. A proposed solution using Monte Carlo Tree Search for managing large-scale Partially Observable Markov Decision Processes is detailed in [41]. As well as this, the problem suffers from combinatorial explosion, meaning the problem quickly becomes intractable, even with moderate planning horizons. An efficient way of searching the action space has been proposed in [10] and a distributed approach to non-myopic planning for multiple targets in [33]. Non-myopic planning has also been used for the control of a single pan-tilt-zoom camera using information theoretic drivers in [39]. A related problem to non-myopic sensor management is the control of an unknown number of interceptors to rendezvous with a given target at a given time [11].

In this paper, we address the sensor management problem by considering a cost function based on a metric for sets of targets. A sensor management algorithm based on the optimal sub-pattern assignment metric was proposed in [18]. In this work, we use the generalised optimal sub-pattern assignment (GOSPA) metric [34]. The GOSPA metric penalises for the localisation error for properly detected targets, the missed targets error and the false targets error [15], which are concepts of interest in traditional multi-target tracking performance evaluation [14]. The GOSPA metric combines these three quantities in a mathematically principled manner providing a cost function that can be used to quantitatively measure performance. The GOSPA localisation error resembles the (unnormalised) multiple object tracking precision score in [5]. The GOSPA metric has been used in track-before-detect sensor management for Bernoulli filtering in [46] and in a non-myopic sample-based approximation for Bernoulli filtering in [20]. An analysis of the favourable properties of the GOSPA metric compared to other metrics for sets of targets in the context of sensor management is provided in [15].

In this paper, we extend the work from [24] to include non-myopic planning, using GOSPA as a driver of performance in a Gaussian Bernoulli setting. Specifically, we propose an upper bound on the mean square GOSPA (MSGOSPA) as a cost function to assign a cost to each available action. We use this bound as it is closed-form for linear-Gaussian systems and computationally efficient to calculate. Then, we develop a Monte Carlo Tree Search (MCTS) algorithm [8] that enables us to solve the non-myopic planning problem in a computationally efficient manner. This algorithm is benchmarked against an information theoretic approach - using the KL divergence. Preliminary results were provided

in the conference version of this paper in [24].

In summary, the contributions of this paper are:

- 1) A sensor management framework for Bernoulli filtering based on GOSPA, suitable for myopic and non-myopic planning.
- 2) The development of a closed form cost function for sensor management based on an upper bound of the MS-GOSPA error for Gaussian single-target distributions.
- 3) A computationally efficient implementation of the planning algorithm based on an MCTS method
- 4) An approximation of the expected probability of detection based on importance sampling for the case in which sensors have a circular FOV with a constant probability of detection.

The rest of the paper is organised as follows. Section II defines the problem of sensor management, Section III details the non-myopic Gaussian Bernoulli sensor management problem, Section IV explains the implementation of the MCTS and how it is applied to this problem, Section V provides the parameters and results of the conducted simulations and Section VI provides concluding statements and planned avenues for future developments in this work.

II. PROBLEM FORMULATION & BACKGROUND

In this section, we provide the sensor management problem formulation and the required background. In particular, in Section II-A, we introduce the dynamic and measurement models for Bernoulli filtering. In Section II-B, we outline the Bernoulli filtering recursion. In Section II-C, we review the GOSPA metric. In Section II-D, we discuss non-myopic planning using the time-discounted predicted MSGOSPA error.

A. Bernoulli Dynamic & Measurement Model

In a Bernoulli model, the target may or may not be present in the surveillance area at a given time-step k . That is, the multi-target state at time-step k is a set X_k that can either be empty ($X_k = \emptyset$) or a singleton ($X_k = \{x_k\}$) where $x_k \in \mathbb{R}^{n_x}$ is the single-target state [31].

The dynamics of a Bernoulli Markov process are characterised by the multi-target transition density $\phi_{k|k-1}(X_k|X_{k-1})$. For $X_{k-1} = \emptyset$, the transition density is

$$\phi_{k|k-1}(X_k|\emptyset) = \begin{cases} 1 - p^B & X_k = \emptyset \\ p^B \cdot b_{k|k-1}(x_k) & X_k = \{x_k\} \\ 0 & |X_k| \geq 2 \end{cases} \quad (1)$$

where p^B is the probability of birth, $b_{k|k-1}(x_k)$ is the single-target birth density at time-step k and $|X_k|$ is the cardinality of the state set.

For $X_{k-1} = \{x_{k-1}\}$, the transition density is

$$\phi_{k|k-1}(X_k|\{x_{k-1}\}) = \begin{cases} 1 - p^S & X_k = \emptyset \\ p^S \cdot \pi_{k|k-1}(x_k|x_{k-1}) & X_k = \{x_k\} \\ 0 & |X_k| \geq 2 \end{cases} \quad (2)$$

where p^S is the probability of survival and $\pi_{k|k-1}(x_k|x_{k-1})$ is the single-target transition density. The birth density contains information on where a new target could appear, and the single-target transition density contains information on how the present target moves.

The sensor has the ability to select a sensing mode $a_k \in \mathbb{A}$ to sense the environment at each time-step k , where \mathbb{A} is a finite set with all of the available sensing modes. At each time-step, a target $x \in X_k$ has the possibility of being detected with a probability of detection $p_{a_k}^D(\cdot)$. A target generated measurement z is then produced with a linear Gaussian density $l(z|x) = \mathcal{N}(z; H_{a_k}x + b_{a_k}, R_{a_k})$, in which H_{a_k} is the observation matrix, R_{a_k} is the observation noise matrix and b_{a_k} is a bias term. The notation $\mathcal{N}(z; \hat{z}, S)$ denotes a Gaussian density, evaluated at z , and parameterised by \hat{z} and S - a mean and a covariance matrix respectively. Clutter is generated by a Poisson point process with clutter rate (intensity) $\lambda_c(\cdot)$. The set of measurements at time-step k , which can contain both clutter and a target generated measurement is denoted Z_k .

B. Bernoulli Filtering

In Bernoulli filtering, both the predicted and posterior densities are Bernoulli densities of the form

$$f_{k|k'}(X_k) = \begin{cases} r_{k|k'} p_{k|k'}(x_{k-1}) & X_k = \{x_k\} \\ 1 - r_{k|k'} & X_k = \emptyset \\ 0 & |X_k| \geq 2 \end{cases} \quad (3)$$

where $k' \in \{k-1, k\}$ with $k' = k-1$ for the predicted density and $k' = k$ for the posterior density, $p_{k|k'}(\cdot)$ is the single-target density and $r_{k|k'}$ is the probability of existence.

The Bernoulli filtering recursion propagates the probability of existence and the single-target density. The prediction equations are given in [38], see Eqs. (28) and (29). The update equations are given by Eqs. (56), (57) and (59) in [38] and have not been repeated here for brevity.

C. The GOSPA metric

Given two sets of targets X and Y , an assignment set γ between them has the following properties $\gamma \subseteq \{1, \dots, |X|\} \times \{1, \dots, |Y|\}$, $(i, j), (i', j') \in \gamma \implies j = j'$ and $(i, j), (i', j) \in \gamma \implies i = i'$. The last two properties ensure that each target is assigned at most once. Given the parameters $\alpha = 2$, maximum localisation error $c > 0$, $p > 0$ and a base metric in the single-target space $d(\cdot, \cdot)$, the GOSPA metric is [34]

$$d_p^{(c,2)}(X, Y) = \min_{\gamma \in \Gamma} \left(\sum_{(i,j) \in \gamma} d^p(x_i, y_j) + \frac{c^p}{2} (|X| + |Y| - 2|\gamma|) \right)^{1/p} \quad (4)$$

where $d^p(\cdot)$ is the localisation error to the p -th power. In a target-tracking scenario, the sets X and Y represent the ground truth and estimated set, respectively. Then, $|X| - |\gamma|$ is the number of missed targets and $|Y| - |\gamma|$ is the number of false targets.

For notational simplicity, in the rest of the paper, we drop the superindices and subindices in the GOSPA metric and just denote it as $d(X, Y)$. We also assume that $p = 2$ and that the base metric is the Euclidean metric.

D. Non-myopic Planning using the time-discounted predicted MSGOSPA Error

In non-myopic sensor management, we optimise over a policy that minimises the predicted cost over multiple future time-steps [27, Chapter 7]. All available information up to time-step $k' \geq k$ for sensor management at time-step k is denoted as

$$\mathcal{I}_{k'} = \begin{cases} (f_{k|k-1}(\cdot)) & k' = k \\ (f_{k'|k'-1}(\cdot), a_{k:k'-1}, Z_{k:k'-1}) & k' \geq k \end{cases} \quad (5)$$

where $a_{k:k'-1} = (a_k, \dots, a_{k'-1})$ and $Z_{k:k'} = (Z_k, \dots, Z_{k'-1})$ denote the sequences of actions and measurement sets from time-step k to $k' - 1$, respectively. The agent then makes decisions, considering the dynamic and measurement models, according to a deterministic policy $\mu_{k'}(\cdot)$ that maps the available information to the next action such that

$$a_{k'} = \mu_{k'}(\mathcal{I}_{k'}) \quad (6)$$

Considering a planning horizon up to time-step K , with a length of $K - k + 1$, the sequence of policies up to the planning horizon is denoted by $\mu_{k:K}(\cdot) = (\mu_k(\cdot), \dots, \mu_K(\cdot))$. Including a decay factor $\lambda \in (0, 1]$, for GOSPA-driven sensor management, the policy is chosen to minimise [27, Eq. (7.6)]

$$J_{\mu_{k:K}}(\cdot) = E_{\mu_{k:K}(\cdot)} \left[\sum_{k'=k}^K \lambda^{k'-k} d^2 \left(X_{k'}, \hat{X}_{k'}(a_{k:k'}, Z_{k:k'}) \right) \right] \quad (7)$$

where the expectation is taken with respect to the joint probability density of $(X_k, \dots, X_K, Z_k, \dots, Z_K)$ under the policy $\mu_{k:K}(\cdot)$, and $\hat{X}_{k'}(a_{k:k'}, Z_{k:k'})$ is the optimal MSGOSPA estimator at time-step k' .

The optimal policy is then

$$\mu_{k:K}^*(\cdot) = \arg \min_{\mu_{k:K}(\cdot)} J_{\mu_{k:K}}(\cdot) \quad (8)$$

and the minimum value of the cost is

$$J_{\mu_{k:K}}^*(\cdot) = \min_{\mu_{k:K}(\cdot)} J_{\mu_{k:K}}(\cdot) \quad (9)$$

The minimum value of the cost can also be written more explicitly as the nested minimisations in (10)-(11), where each minimisation provides the optimal action at a time-step for each possible sequence of past measurements and actions. The integrals in (11) correspond to set integrals in [31], which are reviewed in Appendix A. The terms in (11) are defined as $f_{k|k-1}^m(\cdot; a_k)$ being the predicted density of the measurements for action a_k and $f_{k|k}(\cdot|Z_k, a_k)$ is the posterior density given action a_k and measurement set Z_k . These two densities are explained in more detail in Sections III-B and III-C, respectively. The nested expectations can then be written

$$\begin{aligned}
J_{\mu_{k,K}^*}(\cdot) &= \min_{a_k} E_{Z_k; a_k} \left[d^2 \left(X_k, \hat{X}_k(a_k, Z_k) \right) \right. \\
&\quad + \lambda \min_{a_{k+1}} E_{Z_{k+1}|Z_k; a_{k:k+1}} \left[d^2 \left(X_{k+1}, \hat{X}_{k+1}(a_{k:k+1}, Z_{k:k+1}) \right) \right. \\
&\quad \left. \left. + \dots + \lambda^{K-k} \min_{a_K} E_{Z_K|Z_{k:K-1}; a_{k:K}} \left[d^2 \left(X_K, \hat{X}_K(a_{k:K}, Z_{k:K}) \right) \dots \right] \right] \right]. \tag{10}
\end{aligned}$$

$$\begin{aligned}
&= \min_{a_k} \int f_{k|k-1}^m(Z_k; a_k) \left[\int d^2 \left(X_k, \hat{X}_k(a_k, Z_k) \right) f_{k|k}(X_k | Z_k; a_k) \delta X_k \right. \\
&\quad + \lambda \min_{a_{k+1}} \int f_{k+1|k}^m(Z_{k+1}|Z_k; a_{k:k+1}) \left[\int d^2 \left(X_{k+1}, \hat{X}_{k+1}(a_{k:k+1}, Z_{k:k+1}) \right) f_{k+1|k+1}(X_{k+1} | Z_{k:k+1}; a_{k:k+1}) \delta X_k \right. \\
&\quad \left. \left. + \dots + \lambda^{K-k} \min_{a_K} \int f_{K|K-1}^m(Z_K|Z_{k:K-1}; a_{k:K}) \right. \right. \\
&\quad \left. \left. \left[\int d^2 \left(X_K, \hat{X}_K(a_{k:K}, Z_{k:K}) \right) f_{K|K}(X_K | Z_{k:K}; a_{k:K}) \delta X_K \right] \delta Z_K \dots \right] \delta Z_{k+1} \right] \delta Z_k. \tag{11}
\end{aligned}$$

in a Bellman-type equation using the value function [27]. That is, the value function at the final time-step K is

$$\begin{aligned}
V_K(Z_{k:K-1}, a_{k:K-1}) &= \\
\min_{a_K} E_{Z_K|Z_{k:K-1}, a_{k:K-1}} \left[d^2 \left(X_K, \hat{X}_K(a_{k:K}, Z_{k:K}) \right) \right] \tag{12}
\end{aligned}$$

where it should be noted that the value function depends on previous measurements and actions.

For $k' \in \{k, k+1, \dots, K-1\}$, the value function can be computed recursively backwards via

$$\begin{aligned}
V_{k'}(Z_{k:k'-1}, a_{k:k'-1}) &= \\
\min_{a_{k'}} E_{Z_{k'}|Z_{k:k'-1}, a_{k:k'}} \left[d^2 \left(X_{k'}, \hat{X}_{k'}(a_{k:k'}, Z_{k:k'}) \right) \right. \\
&\quad \left. + \lambda^{k'+1-k} V_{k'+1}(Z_{k:k'}; a_{k:k'}) \right] \tag{13}
\end{aligned}$$

A special case of the non-myopic planning can be considered in which there is no multi-step lookahead, either setting $K = k$ or $\lambda = 0$ in (7). The actions decided by the sensor are informed only by the predictions one time step ahead of the current time step. This is known as myopic planning and results in this optimal action at time step k [19].

$$\begin{aligned}
a_k^* &= \operatorname{argmin}_{a_k} E \left[d^2 \left(X_k, \hat{X}_k(a_k, Z_k) \right); a_k \right] \\
&= \operatorname{argmin}_{a_k} \int \left[\int d^2 \left(X_k, \hat{X}_k(a_k, Z_k) \right) \right. \\
&\quad \left. f_{k|k}(X_k | Z_k; a_k) \delta X_k \right] f_{k|k-1}^m(Z_k; a_k) \delta Z_k \tag{14}
\end{aligned}$$

III. NON-MYOPIC GAUSSIAN BERNOULLI SENSOR MANAGEMENT

This section presents a sensor management algorithm for Bernoulli filtering based on the Gaussian distributions and the GOSPA metric. The assumptions of the sensor management algorithm are

- 1) The clutter intensity $\lambda_c(\cdot)$ is zero.
- 2) We either detect zero measurements $Z_k = \emptyset$ or one measurement $Z_k = \{z_k\}$ at the predicted mean.
- 3) We only consider the component in the Gaussian mixture of the predicted single-target density with the highest associated weight.

- 4) The probability of detection is approximated as a constant given by its predicted value.
- 5) We use a computationally efficient upper bound for the resulting MSGOSPA error.

The rest of the section is organised as follows. Section III-A presents the Gaussian predicted density, Section III-B presents the predicted measurement density, Section III-C presents the updated Bernoulli density for both cases where a measurement is received, and not received, Section III-D presents the upper bound on the MSGOSPA error and Section III-E presents the resulting Bellman equation.

A. Gaussian Predicted Density

We first explain the form of the predicted density. Under Assumption 3), the predicted density is Bernoulli whose density is given by (3) and where the single-target density is Gaussian where

$$p_{k|k-1}(x_k) = \mathcal{N}(x_k; \bar{x}_{k|k-1}, P_{k|k-1}) \tag{15}$$

where $\bar{x}_{k|k-1}$ is the predicted mean and $P_{k|k-1}$ is the predicted covariance.

B. Predicted Measurement Density

Using Assumption 4), the probability of detection is approximated as

$$\begin{aligned}
\bar{p}_{a_k}^D(\bar{x}_{k|k-1}, P_{k|k-1}) &= E[p_{a_k}^D(x)] \\
&= \int p_{a_k}^D(x) \mathcal{N}(x; \bar{x}_{k|k-1}, P_{k|k-1}) dx \tag{16}
\end{aligned}$$

It can be noted here that the integral in (16) is over the single-target space \mathbb{R}^{n_x} . Additionally, using Assumption 1), the predicted density of the measurement is Bernoulli with

$$\begin{aligned}
f_{k|k-1}^m(Z_k; a_k) &\simeq \\
\begin{cases} \bar{p}_{a_k}^D(\bar{x}_{k|k-1}, P_{k|k-1}) r_{k|k-1} \mathcal{N}(z_k; \hat{z}_{a_k}, S_{a_k}) & Z_k = \{z_k\} \\ 1 - r_{k|k-1} \bar{p}_{a_k}^D(\bar{x}_{k|k-1}, P_{k|k-1}) & Z_k = \emptyset \end{cases} \tag{17}
\end{aligned}$$

where the predicted measurement and its covariance matrix are

$$\hat{z}_{a_k} = H_{a_k} \bar{x}_{k|k-1} + b_{a_k} \quad (18)$$

$$S_{a_k} = H_{a_k} P_{k|k-1} H_{a_k}^T + R_{a_k} \quad (19)$$

C. Gaussian Posterior

Considering Assumption 2), we only need to consider two cases to compute the posterior: either there is a target-generated measurement $Z_k = \{\hat{z}_{a_k}\}$, or not $Z_k = \emptyset$. Using the Bernoulli update [24, (6)-(8)] for $\lambda_c(\cdot) \rightarrow 0$, we obtain the updated parameters.

1) For $Z_k = \emptyset$: The updated mean, covariance and probability of existence are

$$\bar{x}_{k|k,a_k}^0 = \bar{x}_{k|k-1} \quad (20)$$

$$P_{k|k,a_k}^0 = P_{k|k-1} \quad (21)$$

$$r_{k|k,a_k}^0 = \frac{(1 - \bar{p}_{a_k}^D(\bar{x}_{k|k-1}, P_{k|k-1}))r_{k|k-1}}{1 - r_{k|k-1} + (1 - \bar{p}_{a_k}^D(\bar{x}_{k|k-1}, P_{k|k-1}))r_{k|k-1}} \quad (22)$$

2) For $Z_k = \{\hat{z}_{a_k}\}$: Under Assumption 1), the updated mean, covariance and probability of existence are [24, App. A]

$$\bar{x}_{k|k,a_k}^1 = \bar{x}_{k|k-1} \quad (23)$$

$$P_{k|k,a_k}^1 = P_{k|k-1} - P_{k|k-1} H_{a_k}^T (S_{a_k})^{-1} H_{a_k} P_{k|k-1} \quad (24)$$

$$r_{k|k,a_k}^1 = 1 \quad (25)$$

The superscript 0 in the updated Bernoulli parameters denote a misdetection hypothesis (no measurement received) and superscript 1 denotes a measurement hypothesis (measurement received)

D. Upper Bound on the MSGOSPA error

Calculating the MSGOSPA error is intractable, and therefore we need to resort to approximations for its use in sensor management. This section provides a closed-form upper bound of the MSGOSPA error in linear Gaussian systems that is fast to calculate and suitable for sensor management.

Given an updated Bernoulli density with parameters (20)-(24), let us consider the following estimator of the set of targets

$$\hat{X}(a_k, Z_k) = \begin{cases} \{\bar{x}_{k|k,a_k}^{j|Z_k}\} & r_{k|k,a_k}^{j|Z_k} \geq \Gamma_d \\ \emptyset & r_{k|k,a_k}^{j|Z_k} < \Gamma_d \end{cases} \quad (26)$$

where Γ_d is the detection threshold. That is, $\hat{X}(a_k, Z_k)$ estimates a target located at the posterior mean if the updated probability of existence is greater than Γ_d and an empty set if the probability of existence is lower. Then, the upper bound for the MSGOSPA error for this estimator is provided in Lemma 1 below.

Lemma 1: Let $(r_{k|k,a_k}^j, P_{k|k,a_k}^j)$ be the updated probability of existence and covariance matrix of the target for $|Z_k| =$

$j, j \in \{0, 1\}$. An upper bound on the MSGOSPA error for a given measurement set Z_k is

$$\int d^2 \left(X_k, \hat{X}_k(a_k, Z_k) \right) f_{k|k}(X_k | Z_k; a_k) \delta X_k \leq C(\Gamma_d, r_{k|k,a_k}^{|Z_k|}, P_{k|k,a_k}^{|Z_k|}) \quad (27)$$

where

$$C(\Gamma_d, r_{k|k,a_k}^{|Z_k|}, P_{k|k,a_k}^{|Z_k|}) = \begin{cases} \frac{c^2}{2} r_{k|k,a_k}^{|Z_k|} & r_{k|k,a_k}^{|Z_k|} \leq \Gamma_d \\ \frac{c^2}{2} (1 - r_{k|k,a_k}^{|Z_k|}) & \\ + r_{k|k,a_k}^{|Z_k|} \min \left(\text{tr}(P_{k|k,a_k}^{|Z_k|}), c^2 \right) & r_{k|k,a_k}^{|Z_k|} > \Gamma_d \end{cases} \quad (28)$$

A proof of this lemma is provided in Appendix B.

The upper bound given by Lemma 1 has two entries, depending on whether the updated probability of existence $r_{k|k,a_k}^{|Z_k|}$ is greater than the detection threshold, Γ_d , or not. Interestingly, this depends only on whether there is a detection or not. It does not depend on either the posterior mean or the received measurement itself. The optimal detection threshold can also be obtained from Lemma 1 [24, App. C]

$$\Gamma_d^* = \frac{1}{2 - \min \left(2 \frac{\text{tr}(P_{k|k,a_k}^{|Z_k|})}{c^2}, 1 \right)} \quad (29)$$

Substituting (29) into (28), the MSGOSPA error upper bound for the optimal detection threshold becomes

$$C(r_{k|k,a_k}^{|Z_k|}, P_{k|k,a_k}^{|Z_k|}) = \begin{cases} \frac{c^2}{2} r_{k|k,a_k}^{|Z_k|} & r_{k|k,a_k}^{|Z_k|} \leq \Gamma_d^* \\ \frac{c^2}{2} (1 - r_{k|k,a_k}^{|Z_k|}) & \\ + r_{k|k,a_k}^{|Z_k|} \min \left(\text{tr}(P_{k|k,a_k}^{|Z_k|}), c^2 \right) & r_{k|k,a_k}^{|Z_k|} > \Gamma_d^* \end{cases} \quad (30)$$

E. The Bellman Equation

In this section, we write the Bellman equation (10)-(11) under the assumptions stated at the beginning of Section III. To do so and to simplify the notation in the nested integrals in (11) when we work under these assumptions, we first introduce binary variable $o_k \in \{0, 1\}$ to indicate when we are in a detection hypothesis $o_k = 1$, which implies $Z_k = \{\hat{z}_{a_k}\}$, or in a misdetection hypothesis $o_k = 0$, which implies $Z_k = \emptyset$. Then, $p(o_{k'} | a_{k:k'}, o_{k:k'-1})$ represents the probability of observing a measurement at time-step k' given actions up to time-step k' and past observations and is given by

$$p(o_{k'} | a_{k:k'}, o_{k:k'-1}) = \begin{cases} \bar{p}_{a_k}^D \left(\bar{x}_{k'|k'-1, a_{k:k'-1}}^{o_{k:k'-1}}, P_{k'|k'-1, a_{k:k'-1}}^{o_{k:k'-1}} \right) & o_{k'} = 1 \\ \times r_{k'|k'-1, a_{k:k'-1}}^{o_{k:k'-1}} & \\ 1 - r_{k'|k'-1, a_{k:k'-1}}^{o_{k:k'-1}} & \\ \times \bar{p}_{a_k}^D \left(\bar{x}_{k'|k'-1, a_{k:k'-1}}^{o_{k:k'-1}}, P_{k'|k'-1, a_{k:k'-1}}^{o_{k:k'-1}} \right) & o_{k'} = 0 \end{cases} \quad (31)$$

where the first subscript term of the probability of existence r , mean \bar{x} and covariance P indicates whether it is predicted $k'|k' - 1$ or updated $k'|k'$, the second subscript term denotes the sequence of actions and the superscript includes the sequence of detections/misdetections. The expected MSGOSPA cost at time-step k' for actions $a_{k:k'}$ and observations $o_{k:k'}$ is

$$C(a_{k:k'}, o_{k:k'}) = \begin{cases} \frac{c^2}{2} r_{k'|k', a_{k:k'}}^{o_{k:k'}} & r_{k'|k', a_{k:k'}}^{o_{k:k'}} \leq \Gamma_d^* \\ \frac{c^2}{2} (1 - r_{k'|k', a_{k:k'}}^{o_{k:k'}}) & r_{k'|k', a_{k:k'}}^{o_{k:k'}} > \Gamma_d^* \\ + r_{k'|k', a_{k:k'}}^{o_{k:k'}} \min(\text{tr}(P_{k'|k', a_{k:k'}}^{o_{k:k'}}), c^2) & \end{cases} \quad (32)$$

Then, the Bellman optimisation in (11), given the assumptions stated at the beginning of Section III, can be simplified as indicated in (33). We can see that the internal MSGOSPA integrals in (11) have been substituted by the bound in Lemma 1, (explicitly given by (32)). In addition, the integrals w.r.t. to the measurements in (11) are now sums, as we are working under the assumption of only having two possible measurement values, and their probability values are given by (31). It should be noted that the predicted mean is independent of the value of o_k and the sequence of actions. Therefore, for the mean, we just need to make the (possibly-multi step) prediction $x_{k'|k}$.

IV. MONTE CARLO TREE SEARCH IMPLEMENTATION

Even with the assumptions stated in Section III, the resulting optimisation problem for non-myopic planning (33) is computationally complex for large time horizons or large action spaces. In this section, we propose the use of MCTS to obtain an approximation to the optimal action [6].

MCTS is a selective search algorithm. It incrementally builds a search tree and decides where to explore next based on what it believes to be the most promising avenues. The tree is continually grown until some predefined terminating condition is reached (such as number of iterations). Once this has been reached, the tree returns the best child of the root node, having considered a larger number of actions within the planning horizon. Typically, MCTS is used to maximise the expected reward over an action space, rather than in this case where we minimise an expected cost. However, we can define the cost as the negative of the reward. We proceed to explain the tree structure, the MCTS algorithm and provide an illustrative example on how it works.

A. Tree Structure

The search tree is initialised by creating the root node, which represents the current time-step k , and setting its reward $R = 0$ (or cost $-R = 0$) and visit count $n = 0$. In [41], the tree is viewed as having two different types of nodes, one set corresponding to actions and the other set corresponding to observations. This is due to the MCTS algorithm being applied to a POMDP. The optimal policy is conditioned on both actions and observations, but we present a simplification of this approach with computational advantages, similar to that in

[39]. The simplification we propose and implement is that each node in the tree only represents an action taken at a specific time-step. Each of these action nodes contains the aggregated costs for both receiving a measurement and not (considering and aggregating both observation hypotheses into a single cost) and information on the target state conditioned on past actions. At each update step required in the search tree, we combine the updated Bernoulli density with no measurement and with measurement into a single Bernoulli with a Gaussian single-target density via moment matching, which corresponds to a KL divergence minimisation [13].

Let $r_{k'|k', a_{k:k'}}$, $\bar{x}_{k'|k', a_{k:k'}}$ and $P_{k'|k', a_{k:k'}}$ be the probability of existence, mean and covariance of each node. How these quantities are predicted, updated and merged (after the update with detection and misdetection) is explained in Appendix D. Then, in this setting, each node in the tree contains this information

- Visit count n .
- Expected cost of visiting node $-R$, defined in (34) (not updated by simulation outcomes).
- Expected cost of visiting node across all time-steps $-\bar{R}$ (updated by simulation outcomes using (36)).
- Parent node.
- Set of child nodes J .
- Set of available actions \mathbb{A}_k .
- Target mean $\bar{x}_{k'|k', a_{k:k'}}$.
- Target covariance matrix $P_{k'|k', a_{k:k'}}$.
- Probability of existence $r_{k'|k', a_{k:k'}}$.
- Probability of detection $\bar{p}_{a_k}^D(\bar{x}_{k'|k'-1, a_{k:k'-1}}, P_{k'|k'-1, a_{k:k'-1}})$.
- Node depth in global tree.

The cost of visiting each node $-R$ is the cost considering both hypotheses (receiving a target generated measurement, or not) and is calculated using (31) and (32)

$$\begin{aligned} -R = & \left(1 - r_{k'|k'-1, a_{k:k'-1}} \bar{p}_{a_{k'}}^D \left(\bar{x}_{k'|k'-1, a_{k:k'-1}}, P_{k'|k'-1, a_{k:k'-1}} \right) \right) \\ & C \left(r_{k'|k', a_{k:k'}}^{o_{k'=0}}, P_{k'|k', a_{k:k'}}^{o_{k'=0}} \right) \\ & + \bar{p}_{a_{k'}}^D \left(\bar{x}_{k'|k'-1, a_{k:k'-1}}, P_{k'|k'-1, a_{k:k'-1}} \right) r_{k'|k'-1, a_{k:k'}} \\ & C \left(r_{k'|k', a_{k:k'}}^{o_{k'=1}}, P_{k'|k', a_{k:k'}}^{o_{k'=1}} \right) \end{aligned} \quad (34)$$

where the factors before $C(\cdot, \cdot)$ represent the probability of no detection and detection for the current node in the tree and the superscript terms indicate whether a measurement was received $o_k = 1$ or not $o_k = 0$.

B. MCTS Algorithm

There are four stages to the MCTS algorithm, they are Selection, Expansion, Simulation and Back-propagation [8].

1) *Selection*: In this stage, a node that still has unvisited children is selected. This node will then be used in the next stage, expansion. To select this node, this phase begins at the root node of the tree. Existing nodes are then recursively

$$\hat{J}_{\mu_{k:K}^*}(\cdot) = \min_{a_k} \sum_{o_k \in \{0,1\}} [p(o_k|a_k)C(a_k, o_k) + \lambda \min_{a_{k+1}} \sum_{o_{k+1} \in \{0,1\}} [p(o_{k+1}|a_{k:k+1}, o_k)C(a_{k:k+1}, o_{k:k+1}) + \dots + \lambda^{K-k+1} \min_{a_K} \sum_{o_K \in \{0,1\}} [p(o_K|a_{k:K-1}, o_{k:K-1})C(a_{k:K}, o_{k:K})] \dots]] \quad (33)$$

selected using the Upper Confidence Bound for Trees (UCT) (35) until an existing node is reached, with at least one unvisited child [8]. A child node j of the current node is selected according to

$$\arg \max_{j \in J} \left\{ \bar{R}_j + 2\epsilon \sqrt{\frac{\ln n}{n_j}} \right\} \quad (35)$$

where n_j is the visit count of the child node, n is the visit count of the current node, ϵ is the trade-off parameter between exploration and exploitation, J is the set of children of the current node and \bar{R}_j is the expected reward from visiting the child node, which will be explained in the backpropagation phase (see (36)). The UCT equation (35) considers both the reward of visiting the node and also how many times it has been visited before, with a trade-off between exploration and exploitation, balanced by ϵ . The UCT causes the tree to grow in areas which show high reward, whilst ensuring that it does not get stuck in this area of the search. The average reward \bar{R}_j is updated during the back-propagation stage. It should be noted that, at the beginning, the selection stage will always select the root node until all of its children have been added to the tree.

2) *Expansion*: A new child node j is added to the selected node. This consists of randomly selecting a previously untried action, predicting the target density, generating the synthetic measurement set, calculating the reward of selecting this action and then updating the target density (considering both the measurement and no measurement hypotheses). How both of these hypotheses are considered is described in (61)-(63) in Appendix D. These node statistics are then used to initialise a new node object which is added to the tree.

3) *Simulation*: A simulation is then run, starting from the child node j . This simulation is run in accordance with the roll-out policy, which is often chosen to be a random path of actions taken down the tree until it reaches a pre-specified terminating condition, which we choose to be the planning horizon. The total reward Δ of this action sequence is calculated as the discounted sum of all of the costs in this action sequence, beginning at the root node of the tree, ending at the final node of the simulation (at the planning horizon). The total reward Δ is given by (33), with the associated approximation in calculating the updated Bernoulli density (see Subsection IV-A) for the sequence of actions $a_{k:K}$ that this path in the tree represents. By starting at the root node, there is always a fair comparison of rewards as the sequence of actions is always the same length.

It can be noted here that the nodes that are used to create a path to the planning horizon, from the current child node j are not added to the tree, and therefore they do not have any

node characteristics to update in the back-propagation phase of the MCTS.

4) *Back-propagation*: The visit count n and associated reward \bar{R} of each of the parent nodes that have been used are updated. The visit count is incremented by one for all parent nodes on the path to the current (child) node j . The reward is updated in each node using (36), in which each term refers to the same node that is being updated

$$\bar{R}_{new} = \frac{(\bar{R}_{old} \cdot n) + \Delta}{n + 1} \quad (36)$$

where \bar{R}_{new} is the updated reward associated with this action/node, \bar{R}_{old} is the reward associated with the action/node prior to this back-propagation phase, n is the visit count of the node and Δ is the reward calculated from the simulation phase. It can be noted here that the reward is updated prior to incrementing the visit count.

C. Illustrative Example

As previously discussed, there are four stages to the MCTS algorithm. We will provide an illustrative example of these four stages. At each time-step, consider a sensor with five available actions at each time-step, and therefore a maximum of five child nodes per parent node. The root node represents the time-step k and contains all of the information listed in Section IV.

1) *Selection*: Here, we start at the root node and select a child node based on the UCT criteria set out by (35). As can be seen in Figure 1, the node on the farthest left has been selected. In this example, as the first selected node has unexplored children, we do not need to evaluate the UCT again during this MCTS iteration.

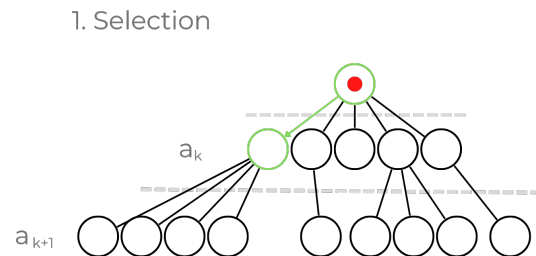


Fig. 1. Selection stage of the MCTS. Top node representing the current time-step with the green nodes indicating which have been selected from the pre-existing tree (black nodes).

2) *Expansion*: Now the parent node has been selected, we add the new child node (representing a sensor action) to the tree in Figure 2. In this case, the parent node only has one child (action) left to be added/considered and therefore no choice of

which child node is required. However, if there were multiple child nodes still to be expanded from the selected node, one would be chosen at random for the expansion. During this phase, the target density is predicted, the ideal measurement set is generated, the cost associated with taking this action (considering both a detection and misdetection hypothesis) is calculated and the target density is then updated (also considering both hypotheses). The node is then added to the tree, initialising its visit count to 0 and cost $-R$ calculated as the expected MSGOSPA (34).

2. Expansion

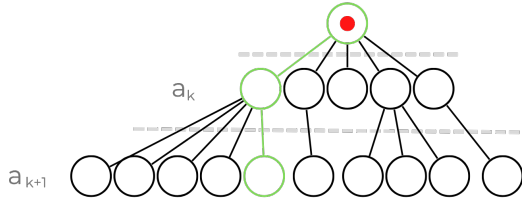


Fig. 2. Expansion stage of the MCTS with green nodes indicating those that have been used to get to the point where the tree has been expanded (lowest green node).

3) *Simulation*: Starting at the most recently added node, a simulation is run down to the planning horizon. The route taken by the simulation is governed by the rollout policy, which is chosen to be a random selection of actions down the search tree until the planning horizon is reached.

This phase is illustrated in Figure 3, it shows an example planning horizon depth of four which determines the maximum search depth of the simulation. As we expanded a node onto the second depth layer of the tree, the simulation phase would only have to look ahead two time-steps to reach the terminating depth. Once the simulation phase has terminated, the cost of this action sequence Δ is taken to be the discounted sum of all actions, starting at the root node, following the path laid out by the selection and simulation phase, down to the planning horizon. The nodes depicted in blue in Figure 3 are not added to the tree and therefore their node characteristics are not updated in the next phase as they are not part of the tree, only the expanded node (lowest green node) has been added to the tree. Note, it is the costs that have not been updated by the other simulation outcomes ($-R$) that are used in the summation to calculate Δ , and not $-R$.

4) *Back-propagation*: Here, the node statistics are updated. The final cost computed in the simulation phase Δ is absorbed into all of the yellow highlighted nodes in Figure 4, in accordance with (36). The visit count of all the yellow highlighted nodes is then incremented by one.

5) *MCTS Example Summary*: Phases 1 - 4 that have been outlined above constitute a single iteration of the MCTS algorithm. The number of MCTS iterations is limited by either a maximum run time or computational constraints. In our case, we have limited the computational budget by defining how large the tree can grow. The higher the budget, the more computation required for each time-step as the tree is growing

3. Simulation

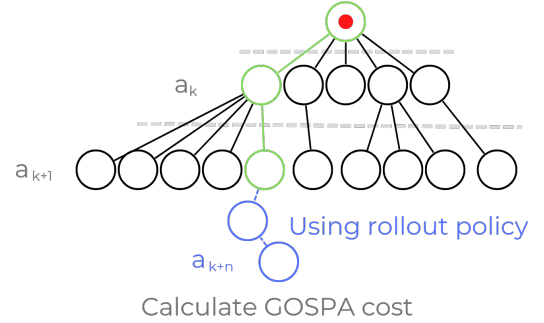


Fig. 3. Simulation phase of the MCTS where the green nodes indicate which nodes have been selected (or expanded - lowest green node) and the blue nodes indicating a random path, as governed by the rollout policy, down to the planning horizon.

4. Backpropagation

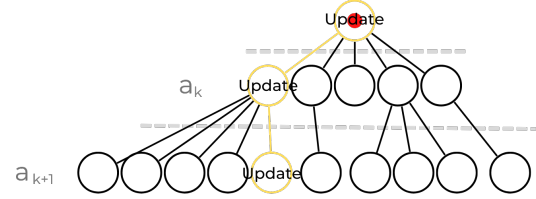


Fig. 4. Back-propagation phase of the MCTS with the yellow nodes indicating which node statistics are set to be updated, starting from the lowest yellow node and propagating back up the tree.

larger each time and looking in more areas of the search space; meaning further into the future.

V. NUMERICAL EXPERIMENTS

In this section, numerical experiments comparing the proposed algorithm for sensor management with a heuristic policy and an information theoretic algorithm are shown. We outline the sensor movement model, obstacles in the surveillance area, the probability of detection approximation and the tracking performance results from the simulations.

In the non-myopic case, the discount factor $\lambda = 0.7$ was applied to the future rewards (33). The chosen rollout policy for the MCTS was a random selection of actions down to a maximum search depth of 10 time-steps. The trade-off parameter was $\epsilon = 0.05$, favouring exploitation over exploration.

A. Target Motion Model

The target motion is modeled using the nearly constant velocity model [2, Chap. 6]. The state vector is $x = [p_x, v_x, p_y, v_y]^T$ where $x_p = [p_x, p_y]^T$ is the position vector

and $x_v = [v_x, v_y]^T$ is the velocity vector. The transition matrix and process noise covariance matrix are

$$F = \begin{bmatrix} 1 & \tau & 0 & 0 \\ 0 & 1 & 0 & 0 \\ 0 & 0 & 1 & \tau \\ 0 & 0 & 0 & 1 \end{bmatrix}; Q = q \cdot \begin{bmatrix} \frac{\tau^3}{3} & \frac{\tau^2}{2} & 0 & 0 \\ \frac{\tau^2}{2} & \tau & 0 & 0 \\ 0 & 0 & \frac{\tau^3}{3} & \frac{\tau^2}{2} \\ 0 & 0 & \frac{\tau^2}{2} & \tau \end{bmatrix} \quad (37)$$

where $\tau = 1$ and $q = 5$. The birth mean vector is $\bar{x}_B = [0.1, 0, 0.1, 0]^T$ and the birth covariance matrix is diagonal and given by $P_B = \text{diag}([1000, 100, 1000, 100]^T)$.

B. Sensor Model

1) *Sensor Movement Model*: We consider a scenario in which the sensor has a limited FOV that can move to keep the target in the FOV. The governing dynamics of the sensor to maintain track of the target is as follows. The sensor has a fixed number of available actions, all equidistant from its current position. Figure 5 shows a sensor with 6 actions. Each action has an associated change in the measurement noise matrix R .

This means that the actions available to the sensor can have an impact on the measurement dynamics, as some actions lead to more uncertainty in the measurement (high R) than others (low R). The sensor has a FOV which is smaller than the area of surveillance region, it is a circular FOV, centred around the sensors current position. The actions are evenly distributed around the circumference of a circle defined by the radius (step size) of the sensor, meaning that the sensor is modelled under constant speed dynamics, capable of travelling a set distance within each discrete time-step k . Figure 5 depicts the sensor movement model if the number of available actions is equal to $|\mathbb{A}| = 6$.

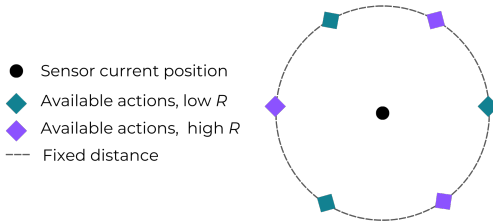


Fig. 5. The sensor movement model where the number of available actions is equal to six.

2) *Sensor Field of View*: Let us consider that the sensor FOV is a circle such that the probability of detection is given by

$$p_{a_k}^D(x) = \begin{cases} p^D & \|x_p - s_{a_k}\| \leq \delta \\ 0 & \|x_p - s_{a_k}\| > \delta \end{cases} \quad (38)$$

where δ is the radius and s_{a_k} is the centre of the FOV, i.e. the sensor position.

The linear measurement model consists of the observation matrix H and observation covariance matrix R . Considering that we measure target position, the H and R matrices are

$$H = \begin{bmatrix} 1 & 0 & 0 & 0 \\ 0 & 0 & 1 & 0 \end{bmatrix}; R = \begin{bmatrix} 10 & 0 \\ 0 & 10 \end{bmatrix} \quad (39)$$

Clutter within the FOV is drawn from a Poisson distribution with a clutter rate $\lambda_c = 1$. Depending on the action selected, the entries in the R matrix vary. We define a ‘low R ’ and a ‘high R ’ as having entries of 10 and 50 along the main diagonal respectively. An example of actions with different R matrices is shown in Figure 5.

C. Obstacles in the Surveillance Area

The surveillance area is defined as square, with the sensor being able to move in accordance to the model defined in Section V-B1. Once the target leaves the surveillance area, the probability of existence is set to zero and the target is considered to have died. Within this surveillance area, we have also introduced some obstacles to make the sensor management problem more challenging. These obstacles have been designed to impact the sensors ability to move, but not the target. An example of this would be if the sensor platform was a ground vehicle and the target an aerial one, encountering different obstacles in their terrain. If the target enters these regions, the movement dynamics are not affected and neither are the measurements.

D. Probability of Detection Approximation

A standard approach to approximate the expected probability of detection $\bar{p}_{a_k}^D(\bar{x}, P)$ in (17) in Gaussian filtering is by using its value at the mean \bar{x} . In this section, we present an approximation with higher accuracy based on importance sampling that improves the sensor management algorithm. Using (38), we can calculate the expected value in (16) such that

$$\bar{p}_{a_k}^D = p^D \int_{\|x_p - s_{a_k}\| \leq \delta} \mathcal{N}(x_p; \bar{x}_{p,k|k-1}, P_{p,k|k-1}) dx_p \quad (40)$$

where $\bar{x}_{p,k|k-1}$ and $P_{p,k|k-1}$ are the predicted mean and covariance matrix of the positional elements and we have dropped the dependence on $\bar{p}_{a_k}^D$ on the predicted mean and covariance for notational simplicity.

It is possible to approximate (40) by drawing samples from the Gaussian density. However, the approximation will be inaccurate if the mass of the Gaussian density is far from the FOV. Therefore, we use importance sampling to improve the accuracy of the estimation. In particular, we write (40) as

$$\bar{p}_{a_k}^D = p^D \int \mathcal{N}(x_p; \bar{x}_{p,k|k-1}, P_{p,k|k-1}) \chi_{\|x_p - s_{a_k}\| \leq \delta}(x_p) dx_p \quad (41)$$

where $\chi_A(\cdot)$ is the indicator function on the set A . To make a uniform density (so that we can draw samples), we need to account for a normalisation factor. In n dimensions, the volume of a n -sphere is

$$V_n(\delta) = \frac{\pi^{n/2}}{\Gamma(n/2 + 1)} \delta^n \quad (42)$$

where $\Gamma(\cdot)$ is the Gamma function. In the standard case in which the position is 2-dimensional, we have

$$V_2(\delta) = \pi \delta^2 \quad (43)$$

which is the surface of the (circular) FOV in (38). Therefore, the uniform density in the field of view is

$$u_{s_{a_k}, \delta}(x_p) = \frac{1}{V_n(\delta)} \chi_{\|x_p - s_{a_k}\| \leq \delta}(x_p) \quad (44)$$

Then, we have

$$\bar{p}_{a_k}^D = p^D V_2(\delta) \int \mathcal{N}(x_p; \bar{x}_{p,k|k-1}, P_{p,k|k-1}) u_{s_{a_k}, \delta}(x_p) dx_p \quad (45)$$

$$\approx p^D V_2(\delta) \frac{1}{I} \sum_{i=1}^I \mathcal{N}(x_{p,i}; \bar{x}_{p,k|k-1}, P_{p,k|k-1}) \quad (46)$$

where $x_{p,i}$ is the i -th sample from $u_{s_{a_k}, \delta}(x_p)$ and I is the number of samples. As I increases, the accuracy of the approximation increases. Specifically, the error of the approximation is $O(I^{-\frac{1}{2}})$ [30].

The expected probability of detection of the target is calculated as a function of both the target and potential sensor positions (actions) at the current time-step k . Figure 6 illustrates the methodology in which sampling is used to calculate an expected probability of detection in one dimension.

Each action (a_k) can be visualised as a window that can see some part of the underlying target distribution. We can calculate an expected probability of detection by calculating the average value of the target distribution which is encapsulated within each window (action). We propose to do this by generating a fixed amount of uniformly distributed samples within each window, evaluate each of these w.r.t. the target distribution, and then take an average of their values. This way, we are able to have a separate probability of detection for each action, based on where the sensor would be relative to the target distribution.

E. Results

In this section, we evaluate the performance of the following algorithms in two scenarios, one in which there are obstacles in the surveillance region, and one where there are none. The first algorithm is the nearest sensor, sensor management algorithm (NS) which can be considered as the heuristic solution to the basic problem where there are no obstacles. The NS algorithm selects the mean of the highest weighted Gaussian component of the predicted density and moves the sensor to the available action that is closest in Euclidean distance to it. This algorithm cannot be extended to non-myopic planning as it does not provide a cost or reward for each action. The second is the myopic GOSPA-driven algorithm, where the performance metric GOSPA is used as a driver for myopic sensor management. The third one is a (myopic) information theoretic sensor management algorithm, using the highest weighted component in the prediction, see Appendix C. Finally, we show three variations of the non-myopic GOSPA-driven algorithm implemented via MCTS, one with a smaller computational budget of 10 nodes, one with a budget of 50 and one with a higher budget of 150 nodes per tree. Note, the smallest budget MCTS has been omitted from the Figures 8 and 10 as to not clutter them.

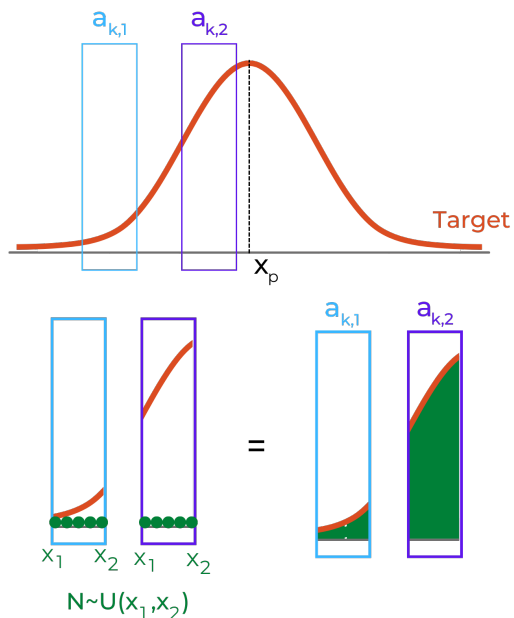


Fig. 6. The methodology to calculate the expected probability of detection, depicted in 1D using 5 samples. The top section denoting the target distribution and two action windows ($a_{k,1}$ and $a_{k,2}$), representing the FOV of two actions. The bottom left figure shows the 5 uniform samples being drawn within the upper and lower limits of each action window. The bottom right figure illustrates the samples being evaluated through the target distribution and an average of them taken.

The root mean square GOSPA (RMS-GOSPA) error at time-step k is

$$\sqrt{\mathbb{E} \left[d^2 \left(X_k, \hat{X}_k \right) \right]} \approx \sqrt{\frac{1}{n} \sum_{i=1}^n d^2 \left(X_k, \hat{X}_{k,i} \right)} \quad (47)$$

where $\hat{X}_{k,i}$ is the estimated set of targets at time-step k in the i -th Monte Carlo (MC) run, and n is the number of Monte Carlo runs. As a measure of performance, we also calculate the RMS-GOSPA error across all time-steps defined as

$$\sqrt{\frac{1}{K} \sum_{k=1}^K \mathbb{E} \left[d^2 \left(X_k, \hat{X}_k \right) \right]} \approx \sqrt{\frac{1}{Kn} \sum_{k=1}^K \sum_{i=1}^n d^2 \left(X_k, \hat{X}_{k,i} \right)} \quad (48)$$

where K is the number of time-steps in the simulation.

The RMS-GOSPA errors were calculated over a simulation length of 300 time-steps and 80 Monte Carlo runs. The GOSPA parameter $c = 2r$ where $r = 40$ and is the radius of the sensors FOV. Two scenarios (obstacles and no obstacles) are simulated with different ground truth trajectories. The planning horizon is set to 5 and therefore the action space has a maximum of 6^5 options to search through.

1) *No Obstacles*: The simulated surveillance region for the no-obstacle simulation is shown in Figure ???. The GOSPA error plots are shown in Figure 8 for the NS algorithm, myopic GOSPA-driven (GD), the information theoretic KL (KL) and MCTS non-myopic GOSPA-driven (MCTS-50, MCTS-150) algorithms. As can be seen from the GOSPA error plots in Figure 8, the MCTS - 150 is the most performant. However,

the performance is not largely greater than the rest of the tested algorithms which provide a computationally less demanding solution. In Table I, we show the RMS-GOSPA errors across all time steps, also including different values of λ for MCTS-10. From these simulations, it can be seen that in such a

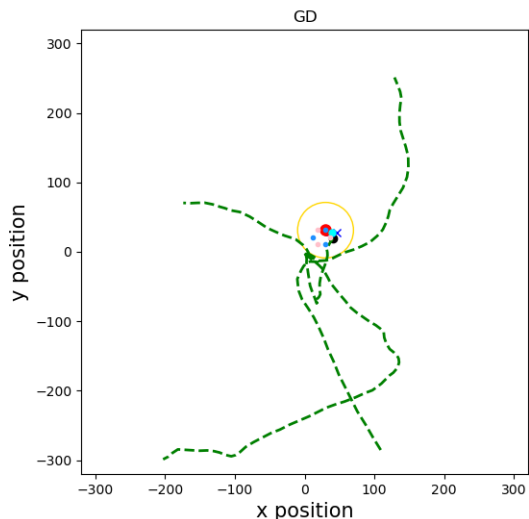


Fig. 7. Scenario snapshot of the GD algorithm in the final MC run when there are no obstacles. The red circle indicates the sensors current position surrounded by the yellow circle which is the sensors current FOV. The pink circles indicate an available action with low R and the blue high R . The black dot is the targets current state, the green lines are legacy tracks where the target has been. The pale blue circle shows the extracted target state from the Bernoulli filter and the dark blue cross shows the measurements received at this time-step. Here there are no major benefits to using a more computationally demanding non-myopic approach.

TABLE I
RMS-GOSPA ERROR FOR EACH ALGORITHM, WITH NO OBSTACLES

Algorithm	Avg. GOSPA Error
NS	45.53
KL	48.15
GD (MCTS $\lambda = 0$)	45.52
MCTS - 10 ($\lambda = 0.7$)	44.46
MCTS - 50 ($\lambda = 0.7$)	44.47
MCTS - 150 ($\lambda = 0.7$)	44.43
MCTS - 10 ($\lambda = 0.5$)	44.39
MCTS - 10 ($\lambda = 0.1$)	42.90

simple scenario, there is no benefit to utilising non-myopic approaches as they are more computationally demanding and are similarly performant compared to simpler algorithms.

2) *Obstacles*: Figure 9, a snapshot of the simulation at time step $k = 210$, illustrates a case where myopic approaches were unable to navigate around an obstacle (shown in grey) and therefore got stuck behind the obstacle when navigating back to the birth location. In contrast, the non-myopic algorithm(s) were able to navigate around the obstacles. The myopic approaches were found to be unable to maintain track of any targets after the point that they got stuck behind an obstacle. This usually happened at around time-step $k = 95$, hence after this point, all of the myopic approaches remain at almost maximum GOSPA error, as shown in Figure 10.

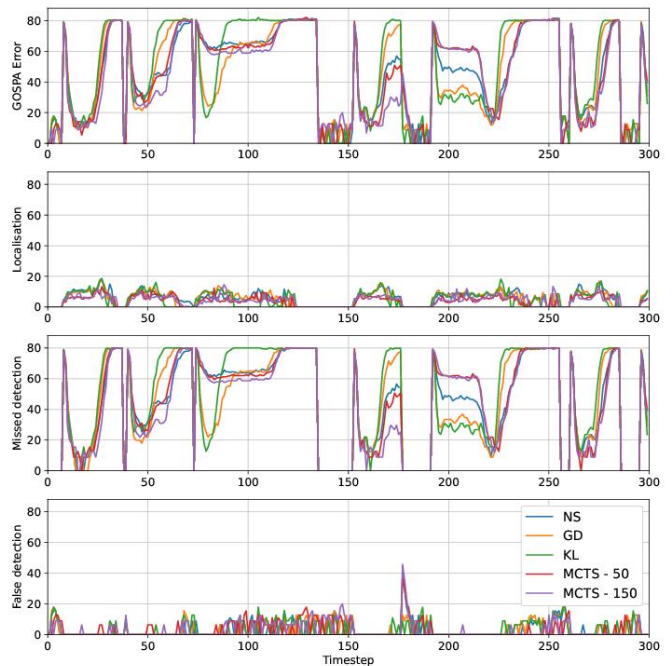


Fig. 8. RMS-GOSPA error breakdown for each time-step where no obstacles are in the surveillance area. Labeled a - d starting from the top plot (a) GOSPA error, (b) localisation error contributions, (c) missed detection error contributions, (d) false detection error contributions

The GOSPA cost broken down into its constituent parts is shown in Figure 10. Peaks in the missed detection error value were usually due to the target appearing in the surveillance area, but are yet to be detected by the sensor. For each simulation the average GOSPA error has been collated in Table II. The approximate average error of the myopic approaches is around 50, whilst the non-myopic approach is around 35. As would be expected, the larger the planning horizon for the non-myopic approaches (i.e. the further into the future the tree could look and grow), the better the tracking performance. We also found that the larger the obstacles were relative to the sensors movement step size, the larger the budget required to enable the non-myopic approach to find a path that navigated around them. Within the simulated scenario, there is no discernible difference in performance between the three non-myopic budgets 10, 50 and 150). This is because for each simulation, the obstacles and sensor movement speed are unchanged. As the budget required to navigate around an obstacle is proportional to the obstacle size and the sensor step size, even a modest budget of 10 is able to plan around the obstacles in the given simulation - resulting in a similar performance of all three differing budgets where $\lambda = 0.7$. For $\lambda = 0.7$ and $\lambda = 0.5$, the algorithm has similar performance. Where $\lambda = 0.1$, the performance of the algorithm drops as it is not sufficiently weighting future costs to be able to navigate around the obstacle.

Table III shows the wall clock time of one 300 time-step simulation and also the time per time-step. The simulations were run on an Intel(R) core (TM) i5-10210U CPU @ 1.6GHz 2.11GHz and the code was written in object-oriented Python.

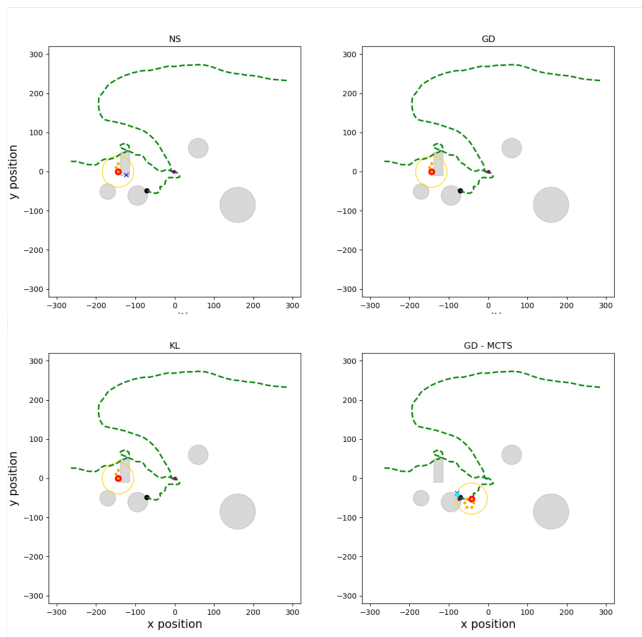


Fig. 9. Snapshot of the final MC run for all algorithms at $k = 210$ where obstacles for the sensor (not the target) are present in the surveillance area (shown as grey shapes). Top left - Nearest Sensor, Top right - GOSPA Driven, Bottom left - Kullback-Leibler Driven, Bottom right - GOSPA Driven MCTS (non-myopic). Here, the obstacles are visualised by the grey shapes. The green dashed line represents the target track and the black dot the target. The red marker is the sensors current location with the yellow circle surrounding it representing the sensors FOV. The light blue dot is the state estimate from the filter and the blue crosses represent measurements (both clutter and target generated). In myopic approaches, the sensor gets stuck in an obstacle and loses the target. The non-myopic GOSPA-driven approach can navigate around the obstacle and keep the target in the FOV.

TABLE II
RMS-GOSPA ERROR FOR EACH ALGORITHM, WITH OBSTACLES

Algorithm	Avg. GOSPA Error
NS	51.67
KL	51.14
GD (MCTS $\lambda = 0$)	50.19
MCTS - 10 ($\lambda = 0.7$)	35.81
MCTS - 50 ($\lambda = 0.7$)	35.52
MCTS - 150 ($\lambda = 0.7$)	35.01
MCTS - 10 ($\lambda = 0.5$)	34.31
MCTS - 10 ($\lambda = 0.1$)	48.79

As expected, myopic approaches have shorter run times, and we can control the computational complexity of MCTS via its computational budget.

VI. CONCLUSION

In this paper, we have proposed a framework for both myopic and non-myopic GOSPA driven sensor management for Bernoulli filtering, a suitable approximation for implementing the planning algorithm based on Gaussian single-target distributions and an upper bound on the MSGOSPA error, and the development of an MCTS method to efficiently conduct non-myopic GOSPA driven sensor management.

We have shown that in a Bernoulli scenario where there are no obstacles, the GD algorithm performs similarly to

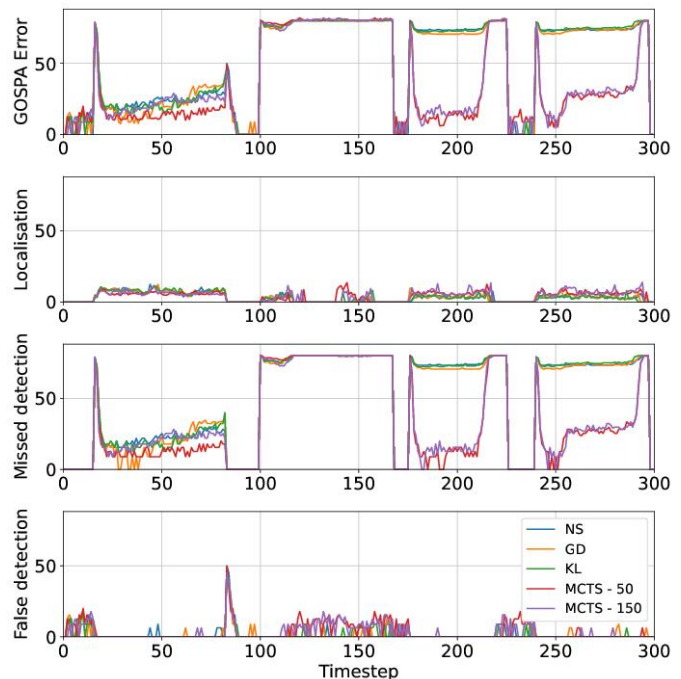


Fig. 10. RMS-GOSPA error breakdown for each time-step where obstacles are in the surveillance area. Labeled a - d starting from the top plot (a) GOSPA error, (b) localisation error contributions, (c) missed detection error contributions, (d) false detection error contributions.

TABLE III
WALL CLOCK COMPUTATION TIME FOR EACH ALGORITHM, WITH OBSTACLES

Algorithm	Avg. time [s]	Avg. time per time-step [s]
NS	13.6	0.05
KL	36.24	0.12
GD	40.3	0.13
MCTS - 10	64.0	0.21
MCTS - 50	220.4	0.73
MCTS - 150	561.9	1.87

the heuristic solution to the problem (NS). We have also shown that the metric driven approach is more performant than an information theoretic approach (KL). We have also demonstrated, and provided a detailed summary of, how non-myopic sensor management can be conducted using an MCTS with GOSPA as a driver, and provided a scenario in which there is a clear benefit to planning non-myopically.

In future work, we plan to extend this work to include multiple targets, using Poisson multi-Bernoulli mixture filters [6], [7]. Another line of future research is to develop reinforcement learning algorithms in combination with Bayesian multi-target tracking algorithms. Another area to explore in further work is to implement parallelised versions of the MCTS algorithm to improve computation time, such as those described in [9].

REFERENCES

- [1] E. H. Aoki, A. Bagchi, P. Mandal, and Y. Boers. A theoretical look at information-driven sensor management criteria. In *International Conference on Information Fusion*, pages 1180–1187, 2011.
- [2] Y. Bar-Shalom, X. Li, and T. Kirubarajan. *Estimation with Applications to Tracking and Navigation: Theory, Algorithms and Software*. 01 2004.

$$\begin{aligned}
r_{k|k,a_k}^1 &= \frac{1 - \bar{p}_{a_k}^D(\bar{x}_{k|k-1}, P_{k|k-1}) \left(1 - \frac{\mathcal{N}(z; \hat{z}_{a_k}, S_{a_k})}{\lambda_c(z)}\right)}{1 - r_{k|k-1} \bar{p}_{a_k}^D(\bar{x}_{k|k-1}, P_{k|k-1}) \left(1 - \frac{\mathcal{N}(z; \hat{z}_{a_k}, S_{a_k})}{\lambda_c(z)}\right)} r_{k|k-1} \\
&= \frac{\lambda_c(z) - \bar{p}_{a_k}^D(\bar{x}_{k|k-1}, P_{k|k-1}) (\lambda_c(z) - \mathcal{N}(z; \hat{z}_{a_k}, S_{a_k}))}{\lambda_c(z) - r_{k|k-1} \bar{p}_{a_k}^D(\bar{x}_{k|k-1}, P_{k|k-1}) (\lambda_c(z) - \mathcal{N}(z; \hat{z}_{a_k}, S_{a_k}))} \quad (49)
\end{aligned}$$

- [3] M. Beard, B.-T. Vo, B.-N. Vo, and S. Arulampalam. Void probabilities and Cauchy-Schwarz divergence for generalized labeled multi-Bernoulli models. *IEEE Transactions on Signal Processing*, 65(19):5047–5061, Oct. 2017.
- [4] K. L. Bell, C. J. Baker, G. E. Smith, J. T. Johnson, and M. Rangaswamy. Cognitive radar framework for target detection and tracking. *IEEE Journal of Selected Topics in Signal Processing*, 9(8):1427–1439, Dec. 2015.
- [5] K. Bernardin and R. Stiefelwagen. Evaluating multiple object tracking performance: The CLEAR MOT metrics. *EURASIP J. Image Video Process.*, 2008, 2008.
- [6] P. Boström-Rost, D. Axehill, and G. Hendeby. Sensor management for search and track using the Poisson multi-Bernoulli mixture filter. *IEEE Transactions on Aerospace and Electronic Systems*, 57(5):2771–2783, 2021.
- [7] P. Boström-Rost, D. Axehill, and G. Hendeby. PMBM filter with partially grid-based birth model with applications in sensor management. *IEEE Transactions on Aerospace and Electronic Systems*, 58(1):530–540, 2022.
- [8] C. B. Browne, E. Powley, D. Whitehouse, S. M. Lucas, P. I. Cowling, P. Rohlfshagen, S. Tavener, D. Perez, S. Samothrakis, and S. Colton. A survey of Monte Carlo tree search methods. *IEEE Transactions on Computational Intelligence and AI in Games*, 4(1):1–43, 2012.
- [9] G. M. J. B. Chaslot, M. H. M. Winands, and H. J. van den Herik. Parallel Monte-Carlo tree search. In H. J. van den Herik, X. Xu, Z. Ma, and M. H. M. Winands, editors, *Computers and Games*, pages 60–71, Berlin, Heidelberg, 2008. Springer Berlin Heidelberg.
- [10] A. S. Chhetri, D. Morrell, and A. Papandreou-Suppappola. Efficient search strategies for non-myopic sensor scheduling in target tracking. In *Conference Record of the Thirty-Eighth Asilomar Conference on Signals, Systems and Computers, 2004.*, volume 2, pages 2106–2110 Vol.2, 2004.
- [11] D. E. Clark. Stochastic multi-object guidance laws for interception and rendezvous problems. *IEEE Transactions on Automatic Control*, 67(3):1482–1489, 2022.
- [12] D. Cormack and D. Clark. Tracking small UAVs using a Bernoulli filter. In *2016 Sensor Signal Processing for Defence (SSPD)*, pages 1–5, 2016.
- [13] M. Fontana, A. F. García-Fernández, and S. Maskell. Data-driven clustering and Bernoulli merging for the Poisson multi-Bernoulli mixture filter. *IEEE Transactions on Aerospace and Electronic Systems*, pages 1–14, 2023.
- [14] B. E. Fridling and O. E. Drummond. Performance evaluation methods for multiple-target-tracking algorithms. volume 1481, pages 371–383, 1991.
- [15] A. F. García-Fernández, M. Hernandez, and S. Maskell. An analysis on metric-driven multi-target sensor management: GOSPA versus OSPa. In *2021 IEEE 24th International Conference on Information Fusion (FUSION)*, pages 1–8, 2021.
- [16] S. Gehly, B. A. Jones, and P. Axelrad. Search-detect-track sensor allocation for geosynchronous space objects. *IEEE Transactions on Aerospace and Electronic Systems*, 54(6):2788–2808, 2018.
- [17] A. Gorji and R. Adve. Policy gradient for observer trajectory planning with application in multi-target tracking problems. In *2018 52nd Asilomar Conference on Signals, Systems, and Computers*, pages 2029–2033, 2018.
- [18] A. K. Gostar, R. Hoseinnezhad, A. Bab-Hadiashar, and W. Liu. Sensor-management for multitarget filters via minimization of posterior dispersion. *IEEE Transactions on Aerospace and Electronic Systems*, 53(6):2877–2884, 2017.
- [19] M. Hernandez. Performance bounds for target tracking: computationally efficient formulations and associated applications. In M. Mallick, V. Krishnamurthy, and B. N. Vo, editors, *Integrated tracking, classification and sensor management*. 2013.
- [20] M. Hernandez, A. F. García-Fernández, and S. Maskell. Non-myopic sensor control for target search and track using a sample-based GOSPA implementation. *accepted in IEEE Transactions on Aerospace and Electronic Systems*, 2023.
- [21] M. L. Hernandez, A. Farina, and B. Ristic. PCRLB for tracking in cluttered environments: measurement sequence conditioning approach. *IEEE Transactions on Aerospace and Electronic Systems*, 42(2):680–704, 2006.
- [22] A. O. Hero III, D. A. Castañón, D. Cochran, and K. Kastella. *Foundations and Applications of Sensor Management*. Springer, 2008.
- [23] F. Hoffmann, A. Charlish, M. Ritchie, and H. Griffiths. Sensor path planning using reinforcement learning. In *2020 IEEE 23rd International Conference on Information Fusion (FUSION)*, pages 1–8, 2020.
- [24] G. Jones, A. F. García-Fernández, and P. W. H. Wong. GOSPA-driven Gaussian Bernoulli sensor management. In *26th International Conference on Information Fusion*, pages 1–8, 2023.
- [25] C. Kreucher, A. Hero, K. Kastella, and D. Chang. Efficient methods of non-myopic sensor management for multitarget tracking. In *2004 43rd IEEE Conference on Decision and Control (CDC) (IEEE Cat. No.04CH37601)*, volume 1, pages 722–727 Vol.1, 2004.
- [26] C. M. Kreucher, A. O. Hero III, K. D. Kastella, and M. R. Morelande. An information-based approach to sensor management in large dynamic networks. *Proceedings of the IEEE*, 95(5):978–999, May 2007.
- [27] V. Krishnamurthy. *Partially Observed Markov Decision Processes: From Filtering to Controlled Sensing*. Cambridge University Press, 2016.
- [28] K. A. LeGrand, P. Zhu, and S. Ferrari. Cell multi-Bernoulli (cell-MB) sensor control for multi-object search-while-tracking (SWT). *IEEE Transactions on Pattern Analysis and Machine Intelligence*, 45(6):7195–7207, 2023.
- [29] G. Li, G. Li, and Y. He. Resolvable group target tracking via multi-Bernoulli filter and its application to sensor control scenario. *IEEE Transactions on Signal Processing*, 70:6286–6299, 2022.
- [30] J. S. Liu. *Monte Carlo strategies in scientific computing*. Springer Verlag, New York, Berlin, Heidelberg, 2008.
- [31] R. P. S. Mahler. *Advances in Statistical Multisource-Multitarget Information Fusion*. Artech House, 2014.
- [32] B. Oakes, D. Richards, J. Barr, and J. Ralph. Double deep Q networks for sensor management in space situational awareness. pages 1–6, 07 2022.
- [33] S. Park, Y. Min, J. Ha, D. Cho, and H. Choi. A distributed admm approach to non-myopic path planning for multi-target tracking. *IEEE Access*, 7:163589–163603, 2019.
- [34] A. S. Rahmathullah, A. F. García-Fernández, and L. Svensson. Generalized optimal sub-pattern assignment metric. In *2017 20th International Conference on Information Fusion (Fusion)*, pages 1–8, 2017.
- [35] L. Ren, J. Lu, Z. Wang, Q. Tian, and J. Zhou. Collaborative deep reinforcement learning for multi-object tracking. In V. Ferrari, M. Hebert, C. Sminchisescu, and Y. Weiss, editors, *Computer Vision – ECCV 2018*, pages 605–621, Cham, 2018. Springer International Publishing.
- [36] B. Ristic, S. Arulampalam, and N. Gordon. *Beyond the Kalman Filter: Particle Filters for Tracking Applications*. Artech House, 2004.
- [37] B. Ristic, B. Vo, and D. Clark. A note on the reward function for PHD filters with sensor control. *IEEE Transactions on Aerospace and Electronic Systems*, 47(2):1521–1529, April 2011.
- [38] B. Ristic, B. Vo, B. Vo, and A. Farina. A tutorial on Bernoulli filters: Theory, implementation and applications. *IEEE Transactions on Signal Processing*, 61(13):3406–3430, 2013.
- [39] P. Salvagnini, F. Pernici, M. Cristani, G. Lisanti, A. D. Bimbo, and V. Murino. Non-myopic information theoretic sensor management of a single pan-tilt-zoom camera for multiple object detection and tracking. *Computer Vision and Image Understanding*, 134:74–88, 2015.
- [40] A. A. Saucan, S. Das, and M. Z. Win. On multisensor activation policies for Bernoulli tracking. In *MILCOM 2021 - 2021 IEEE Military Communications Conference (MILCOM)*, pages 795–801, 2021.
- [41] D. Silver and J. Veness. Monte-carlo planning in large pomdps. In J. Lafferty, C. Williams, J. Shawe-Taylor, R. Zemel, and A. Culotta,

editors, *Advances in Neural Information Processing Systems*, volume 23. Curran Associates, Inc., 2010.

- [42] X. Tang, M. Li, R. Tharmarasa, and T. Kirubarajan. Posterior cramer-rao lower bounds for extended target tracking with Gaussian process pmht. In *2019 22th International Conference on Information Fusion (FUSION)*, pages 1–8, 2019.
- [43] R. Tharmarasa, T. Kirubarajan, M. L. Hernandez, and A. Sinha. PCRLB-based multisensor array management for multitarget tracking. *IEEE Transactions on Aerospace and Electronic Systems*, 43(2):539–555, 2007.
- [44] S. Thrun, W. Burgard, and D. Fox. *Probabilistic Robotics*. MIT Press, 2005.
- [45] P. Tichavsky, C. Muravchik, and A. Nehorai. Posterior Cramer-Rao bounds for discrete-time nonlinear filtering. *IEEE Transactions on Signal Processing*, 46(5):1386–1396, 1998.
- [46] L. Úbeda-Medina. *Robust techniques for multiple target tracking and fully adaptive radar*. PhD thesis, Universidad Politecnica de Madrid, 2018.

APPENDIX A SET INTEGRAL

Let $f(\cdot)$ be a real-valued function on the space $\mathcal{F}(\mathbb{R}^{n_x})$, which denotes the set of all the finite subsets of \mathbb{R}^{n_x} . Then, its set integral is defined as [31]

$$\int f(X) \delta X = \sum_{n=0}^{\infty} \frac{1}{n!} \int \dots \int f(\{x_1, \dots, x_n\}) dx_1 \dots dx_n \quad (50)$$

We can see that the set integral sums over all possible set cardinalities, represented by the integer n . Then, for cardinality n , the set integral performs n integrals over the space \mathbb{R}^{n_x} . More details on the set integral are provided for example in [31].

APPENDIX B PROOF OF LEMMA 1

In this Appendix, we provide the proof of Lemma 1. The MSGOSPA error is

$$\begin{aligned} & \int d^2(X_k, \hat{X}(a_k, Z_k)) f_{k|k}(X_k | Z_k; a_k) \delta X_k \\ &= d^2(\emptyset, \hat{X}(a_k, Z_k)) \left(1 - r_{k|k, a_k}^{|Z_k|}\right) \\ &+ r_{k|k, a_k}^{|Z_k|} \int d^2(\{x_k\}, \hat{X}(a_k, Z_k)) p_{k|k}(x_k) dx_k \end{aligned} \quad (51)$$

If $r_{k|k, a_k}^{|Z_k|} \leq \Gamma_d$, we substitute (26) into (51) to obtain

$$\int d^2(X_k, \emptyset) f_{k|k}(X_k | Z_k; a_k) \delta X_k = r_{k|k, a_k}^{|Z_k|} \frac{c^2}{2} \quad (52)$$

which proves the first entry of (28).

If $r_{k|k, a_k}^{|Z_k|} \geq \Gamma_d$, we substitute (26) into (51) to obtain

$$\begin{aligned} & \int d^2(X_k, \hat{X}(a_k, Z_k)) f_{k|k}(X_k | Z_k; a_k) \delta X_k \\ &= \frac{c^2}{2} \left(1 - r_{k|k, a_k}^{|Z_k|}\right) + r_{k|k, a_k}^{|Z_k|} \\ &\times \int \min\left(c^2, \left\|x_k - \bar{x}_{k|k, a_k}^{|Z_k|}\right\|^2\right) \mathcal{N}\left(x_k; \bar{x}_{k|k, a_k}^{|Z_k|}, P_{k|k, a_k}^{|Z_k|}\right) dx_k \end{aligned} \quad (53)$$

Now, we can obtain two upper bounds to the integral in the above expression. Since $\min\left(c^2, \left\|x_k - \bar{x}_{k|k, a_k}^{|Z_k|}\right\|^2\right) \leq c^2$, we first have that

$$\int \min\left(c^2, \left\|x_k - \bar{x}_{k|k, a_k}^{|Z_k|}\right\|^2\right) \mathcal{N}\left(x_k; \bar{x}_{k|k, a_k}^{|Z_k|}, P_{k|k, a_k}^{|Z_k|}\right) dx_k \leq c^2 \quad (54)$$

On the other hand, we have

$$\min\left(c^2, \left\|x_k - \bar{x}_{k|k, a_k}^{|Z_k|}\right\|^2\right) \leq \left\|x_k - \bar{x}_{k|k, a_k}^{|Z_k|}\right\|^2 \quad (55)$$

This inequality implies that

$$\begin{aligned} & \int \min\left(c^2, \left\|x_k - \bar{x}_{k|k, a_k}^{|Z_k|}\right\|^2\right) \mathcal{N}\left(x_k; \bar{x}_{k|k, a_k}^{|Z_k|}, P_{k|k, a_k}^{|Z_k|}\right) dx_k \\ &\leq \int \left\|x_k - \bar{x}_{k|k, a_k}^{|Z_k|}\right\|^2 \mathcal{N}\left(x_k; \bar{x}_{k|k, a_k}^{|Z_k|}, P_{k|k, a_k}^{|Z_k|}\right) dx_k \\ &= \text{tr}\left(P_{k|k, a_k}^{|Z_k|}\right) \end{aligned} \quad (56)$$

Therefore, we can write the inequalities (54) and (56) compactly as

$$\begin{aligned} & \int \min\left(c^2, \left\|x_k - \bar{x}_{k|k, a_k}^{|Z_k|}\right\|^2\right) \mathcal{N}\left(x_k; \bar{x}_{k|k, a_k}^{|Z_k|}, P_{k|k, a_k}^{|Z_k|}\right) dx_k \\ &\leq \min\left(c^2, \text{tr}\left(P_{k|k, a_k}^{|Z_k|}\right)\right) \end{aligned} \quad (57)$$

Substituting this expression into (53), we obtain

$$\begin{aligned} & \int d^2(X_k, \hat{X}(a_k, Z_k)) f_{k|k}(X_k | Z_k; a_k) \delta X_k \\ &\leq \frac{c^2}{2} \left(1 - r_{k|k, a_k}^{|Z_k|}\right) + r_{k|k, a_k}^{|Z_k|} \min\left(c^2, \text{tr}\left(P_{k|k, a_k}^{|Z_k|}\right)\right) \end{aligned} \quad (58)$$

which proves the second entry in (28) and finishes the proof of Lemma 1.

APPENDIX C KULLBACK-LEIBLER DIVERGENCE BETWEEN TWO BERNOULLI GAUSSIAN DENSITIES

For completeness, here we provide the equation used to calculate the KL divergence between two Bernoulli Gaussian densities. In particular, in information-theoretic sensor management, we calculate the KL divergence between the posterior density and the predicted density [26]. Therefore, we can use the following expressions instead of the upper bound on the MSGOSPA cost in Lemma 1 to determine sensor actions.

Let $f_{k|k'}(\cdot)$ with $k' \in \{k, k-1\}$ be the posterior and predicted Bernoulli densities with probability of existence $r_{k|k'}$ and Gaussian single-target density with mean $\bar{x}_{k|k'}$ and covariance matrix $P_{k|k'}$. If the probability of existence $r_{k|k-1} \notin \{0, 1\}$, the KL divergence of $f_{k|k}$ from $f_{k|k-1}$ is given by [13]

$$\begin{aligned} & D_{KL}(f_{k|k} || f_{k|k-1}) \\ &= (1 - r_{k|k-1}) \log \frac{1 - r_{k|k-1}}{1 - r_{k|k}} + r_{k|k-1} \log \frac{r_{k|k-1}}{r_{k|k}} \\ &+ \frac{r_{k|k-1}}{2} \left[\text{tr}\left((P_{k|k})^{-1} P_{k|k-1}\right) - \log \left(\frac{|P_{k|k-1}|}{|P_{k|k}|}\right) - n_x \right. \\ &\quad \left. + (\bar{x}_{k|k} - \bar{x}_{k|k-1})^T (P_{k|k})^{-1} (\bar{x}_{k|k} - \bar{x}_{k|k-1}) \right] \end{aligned} \quad (59)$$

If $r_{k|k-1} = r_{k|k} \in \{0, 1\}$ the KL divergence is

$$\begin{aligned} & D_{KL}\left(f_{k|k} || f_{k|k-1}\right) \\ &= \frac{r_{k|k-1}}{2} \left[\text{tr}\left(\left(P_{k|k}\right)^{-1} P_{k|k-1}\right) - \log\left(\frac{|P_{k|k-1}|}{|P_{k|k}|}\right) - n_x \right. \\ & \quad \left. + (\bar{x}_{k|k} - \bar{x}_{k|k-1})^T (P_{k|k})^{-1} (\bar{x}_{k|k} - \bar{x}_{k|k-1}) \right] \quad (60) \end{aligned}$$

APPENDIX D

PROBABILITY OF EXISTENCE, MEAN AND COVARIANCE IN THE MCTS IMPLEMENTATION

This appendix explains how the target probability of existence, mean and covariance are propagated in the MCTS implementation explained in Section IV. The probability of existence, mean and covariance of the target are predicted using (15). Then for the update, we update them with no measurement using (20)-(22) giving rise to $r_{k'|k', a_{k:k'}}^{o_k=0}$, $\bar{x}_{k'|k', a_{k:k'}}^{o_k=0}$ and $P_{k'|k', a_{k:k'}}^{o_k=0}$.

The update with measurements is carried out with (25)-(24) giving rise to $r_{k'|k', a_{k:k'}}^{o_k=1}$, $\bar{x}_{k'|k', a_{k:k'}}^{o_k=1}$ and $P_{k'|k', a_{k:k'}}^{o_k=1}$.

The two updates (with and without measurements) are merged via KL divergence minimisation as in [13].

$$r_{k'|k', a_{k:k'}} = w^0 \cdot r_{k'|k', a_{k:k'}}^{o_k=0} + w^1 \cdot r_{k'|k', a_{k:k'}}^{o_k=1} \quad (61)$$

$$\bar{x}_{k'|k', a_{k:k'}} = w^0 \cdot \bar{x}_{k'|k', a_{k:k'}}^{o_k=0} + w^1 \cdot \bar{x}_{k'|k', a_{k:k'}}^{o_k=1} \quad (62)$$

$$P_{k'|k', a_{k:k'}} = w^0 \cdot P_{k'|k', a_{k:k'}}^{o_k=0} + w^1 \cdot P_{k'|k', a_{k:k'}}^{o_k=1} \quad (63)$$

where

$$\begin{aligned} w^0 &= 1 - \left(r_{k'|k'-1, a_{k:k'}} \right. \\ & \quad \left. \cdot \bar{p}_{a'_k}^D \left(\bar{x}_{k'|k'-1, a_{k:k'-1}}, P_{k'|k'-1, a_{k:k'-1}} \right) \right) \quad (64) \end{aligned}$$

$$\begin{aligned} w^1 &= r_{k'|k'-1, a_{k:k'}} \\ & \quad \cdot \bar{p}_{a'_k}^D \left(\bar{x}_{k'|k'-1, a_{k:k'-1}}, P_{k'|k'-1, a_{k:k'-1}} \right) \quad (65) \end{aligned}$$

and $r_{k'|k', a_{k:k'}}^{o_k=0}$ is the updated probability of existence in a misdetection hypothesis, $r_{k'|k', a_{k:k'}}^{o_k=1}$ is the updated probability of existence in a detection hypothesis. $\bar{x}_{k'|k', a_{k:k'}}^{o_k=0}$ and $\bar{x}_{k'|k', a_{k:k'}}^{o_k=1}$ are the updated target means for the misdetection and detection hypotheses respectively. $P_{k'|k', a_{k:k'}}^{o_k=0}$ and $P_{k'|k', a_{k:k'}}^{o_k=1}$ are the updated target covariance matrices for the misdetection and detection hypothesis, respectively.